ARTICLES

Journal of Semiconductors
(2023) 44, 082501
doi: 10.1088/1674-4926/44/8/082501

Spin injection into heavily-doped n-GaN via Schottky barrier

Zhenhao Sun[1], Ning Tang[1, 2, †], Shuaiyu Chen[1], Fan Zhang[3], Haoran Fan[4], Shixiong Zhang[1], Rongxin Wang[3], Xi Lin[4], Jianping Liu[3], Weikun Ge[1], and Bo Shen[1, 2]

[1]State Key Laboratory of Artificial Microstructure and Mesoscopic Physics, School of Physics, Peking University, Beijing 100871, China

[2]Frontiers Science Center for Nano-optoelectronics & Collaboration Innovation Center of Quantum Matter, Peking University, Beijing 100871, China

[3]Suzhou Institute of Nano-Tech and Nano-Bionics (SINANO), Chinese Academy of Sciences, Suzhou 215123, China

[4]International Center for Quantum Materials, Peking University, Beijing 100871, China

Abstract: Spin injection and detection in bulk GaN were investigated by performing magnetotransport measurements at low temperatures. A non-local four-terminal lateral spin valve device was fabricated with Co/GaN Schottky contacts. The spin injection efficiency of 21% was achieved at 1.7 K. It was confirmed that the thin Schottky barrier formed between the heavily n-doped GaN and Co was conducive to the direct spin tunneling, by reducing the spin scattering relaxation through the interface states.

Key words: GaN; spin injection; Schottky barrier; magnetoresistance

Citation: Z H Sun, N Tang, S Y Chen, F Zhang, H R Fan, S X Zhang, R X Wang, X Lin, J P Liu, W K Ge, and B Shen, Spin injection into heavily-doped n-GaN via Schottky barrier[J]. *J. Semicond.*, 2023, 44(8), 082501. https://doi.org/10.1088/1674-4926/44/8/082501

1. Introduction

In recent years, the spintronic device has been developed because of its potentials of low power consumption, high computing speed, and high integration compared with traditional electronic devices[1–3]. Nitride wide-bandgap semiconductors represented by GaN are favorable for spintronic device because of the high Curie temperature of the GaN-based diluted magnetic semiconductors and tunable spin-orbit coupling strength[4–6]. To realize GaN-based spintronic devices, efficient spin injection into GaN channel is a prerequisite. Compared with optical spin injection methods[7], electrical spin injection is more difficult because of the conductance mismatch between the ferromagnetic metals and semiconductors[8, 9]. A tunneling barrier such as MgO or Al_2O_3 is raised to solve this problem[10, 11], which has been utilized in GaN-based spin injection structures so far[12–14]. Another technological route is to use a naturally formed Schottky tunneling barrier between the ferromagnetic metals and semiconductors[15, 16]. The Schottky barrier contact has the advantage of convenient technological process, and has therefore become more important for developing GaN-based spintronic devices. Up to now, spin injection based on Schottky tunneling barrier has been used for spin light emitting diodes[17], but has yet to be demonstrated in non-local spin valves based on spin transport.

In this work, a four-terminal lateral spin valve with Schottky tunneling barrier based on bulk GaN was fabricated. The spin injection polarization of 21% was achieved at 1.7 K. It was confirmed that the thin Schottky barrier was conducive to the direct spin tunneling by reducing the spin scattering relaxation through the interface states.

Correspondence to: N Tang, ntang@pku.edu.cn
Received 7 JANUARY 2023; Revised 28 FEBRUARY 2023.

2. Experiment

The lateral ferromagnet-semiconductor spin valve was fabricated upon Si-doped c-plane wurtzite GaN grown by metal-organic chemical vapor deposition (MOCVD). The thickness of the epitaxial GaN layer is 2 μm and the doping density is 1×10^{19} cm^{-3}. The GaN epitaxial wafer was then directly transferred into the chamber of an ultrahigh vacuum magneto-sputtering through an on-line ultra-high-vacuum interconnection system. In this system, the sample was not exposed into atmospheric environment and the possible influence of other factors can be minimized. Next, a 30 nm Co layer and a 30 nm Pt layer were deposited by magneto-sputtering to form the ferromagnetic tunneling injection contacts. The in-plane coercive field of Co film on GaN was measured to be 100 Oe at room temperature. The four-terminal device was initiated by standard UV lithography to define the reference electrode regions. The injector and detector electrode regions were defined by electron beam lithography and the transport channel was designed to be 400 nm. A 20 nm Ti layer and a 100 nm Au layer were deposited by electron beam evaporation to form the pattern mask. Finally, ion beam etching (IBE) was employed to etch the Co/Pt not covered by the Ti/Au mask, and the four-terminal spin valve was then fabricated. As shown in Fig. 1(a), the spin injector and detector have the dimensions of 20×90 and 50×90 μm^2, respectively. Low temperature magnetotransport measurements were performed by an integrated Cryogen-free superconducting magnet system with a ^{3}He sample-in-vacuum insert (TeslatronPT, Oxford instrument). Keithley 2400 source meter, Keysight 33500B waveform generator and a SR830 lock-in amplifier were used to conduct the electrical measurements.

Atomic force microscope (AFM) measurements were performed to ascertain the length and depth of the channel. As shown in Fig. 1(b), the electrode boundaries on both sides of

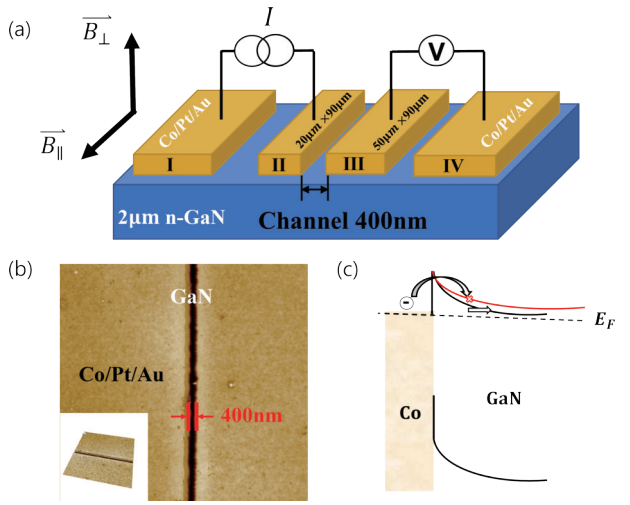

Fig. 1. (Color online) (a) Schematic illustration of the four-terminal non-local measurement scheme (not drawn to scale). (b) AFM image of the GaN channel between injection and detection electrodes. (c) Schematic diagram of Schottky barrier tunneling at various doping densities. A lower doping density of GaN channel (red conduction band case) has a thicker barrier which causes spin polarized electrons being trapped by interface states.

the channel are clear and regular. Due to the extremely slow etching rate of GaN by IBE, the channel depth (the distance from the electrode surface to the channel GaN surface) represents the thickness of the spin injection electrode, which is 80 nm. The spin tunneling layer is Co/Pt (30 nm/30 nm) with a total thickness of 60 nm. Therefore, the 80 nm depth of the channel reveals that the IBE does not damage the Co/Pt spin tunneling layer. The channel length of 400 nm can be clearly seen from the AFM image.

3. Results and discussion

Two-terminal conductance measurements were performed to verify the tunneling process. The DC equivalent circuit can be regarded as a series connection of two backward Schottky junctions, so the *I*–*V* characteristics indicate the tunneling process of the junctions under negative bias as shown in Fig. 1(c). Fig. 2(a) shows the two-terminal *I*–*V* characteristics of the lateral spin valve device at various temperatures. It can be observed that the *I*–*V* characteristics of the GaN/Co Schottky junction exhibit a non-linear and symmetric behavior. Rowell criteria were applied to determine the tunneling process[18]. First, the conductance of the tunneling junctions should have a parabolic dependence on the applied voltage. The inset in Fig. 2(a) shows the differential conductance as a function of the bias voltage, together with a parabolic fit to the curve. Second, the zero-bias conductance should exhibit a weak, insulating-like temperature dependence which is proposed as a definitive confirmation of tunneling[18]. The temperature dependence of the zero-bias conductance is depicted in Fig. 2(b). The conductance shows a weak dependence on temperature, which satisfies the second Rowell criterion. Therefore, the direct tunneling process is dominant in this Schottky barrier.

As shown in Fig. 1(c), a thicker Schottky barrier may trap the spin-polarized electrons, and thus influence the spin transport due to the participation of the localized interface

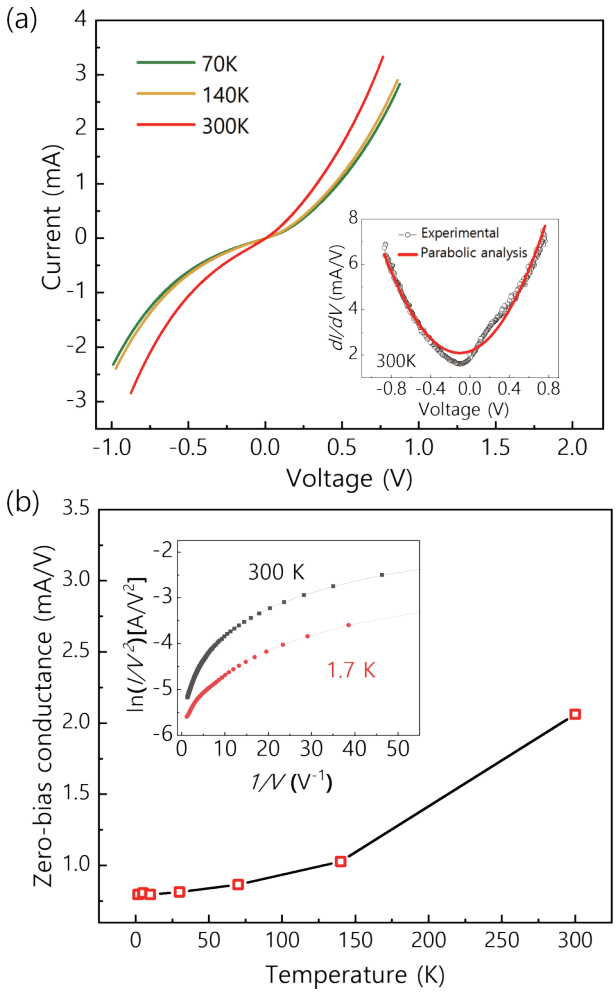

Fig. 2. (Color online) (a) The *I*–*V* characteristics of the injection circuit of the sample at various temperatures. The inset shows the differential conductance as a function of the bias voltage. (b) The zero-bias conductance as a function of temperature. The inset shows the $\ln(I/V^2)$–$1/V$ curves for various temperatures.

states[19]. The width of the Schottky barrier d is expressed as $d = (2\varepsilon\phi_0/eN_D)^{0.5}$, where $\varepsilon, \phi_0, e, N_D$ are the dielectric constant, barrier height, elementary charge and doping density, respectively. As a result, a heavily-doped GaN will have a thinner barrier which is beneficial for the direct tunneling. Moreover, the barrier narrowing related tunneling will participate in the tunneling process when the barrier width is relatively large[20]. The feature of this tunneling (similar to the Fowler-Nordheim tunneling) is an increasing trend of $\ln(I/V^2)$ with an increase in V[21], which can be excluded as shown in the inset of Fig. 2(b), demonstrating an appropriate thin Schottky barrier in our sample. As evidenced by the above two-terminal electrical measurements, the spin polarized electrons can be directly injected into the GaN channel rather than be trapped or scattered by the interface states.

A non-local four-terminal geometry was utilized to investigate the spin injection, spin transport and spin detection in the bulk GaN channel, which could guarantee the validity of the spin related signals. The spurious magnetostatic effects, such as local Hall effects and anisotropic magnetoresistance, can be excluded in this geometry[22–24]. The term "non-local" refers to the fact that the spin-voltage-detection part (Electrodes Ⅲ and Ⅳ) is separated from the charge-current-injec-

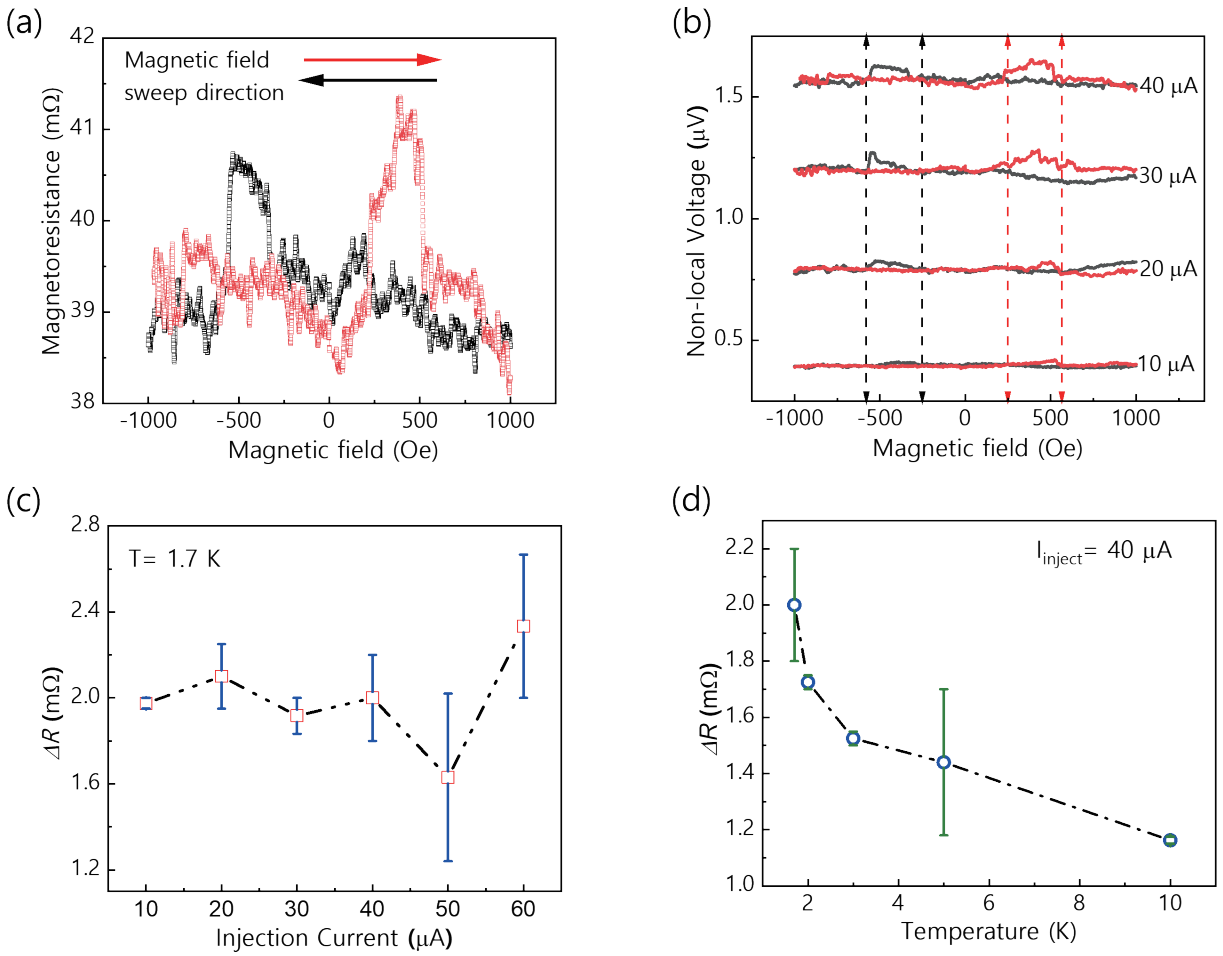

Fig. 3. (Color online) (a) Magnetoresistance as a function of in-plane magnetic field under a constant injection current of I_{inject} = 40 μA at 1.7 K. (b) The injection current-dependent non-local voltage at 1.7 K. The non-local voltage peaks are always restricted in the range of ±(250–600)Oe as surrounded by four corresponding dotted lines. (c) The magnetoresistance difference extracted by non-local measurements at various injection currents. (d) The temperature dependent ΔR under 40 μA injection current.

tion part (Electrodes Ⅰ and Ⅱ) as shown in Fig. 1(a). A constant injection current flows between Electrodes Ⅰ and Ⅱ on the left-hand side of the sample, and then the spin polarized electrons will diffuse beneath the right-hand side electrodes that generate a non-local voltage between the ferromagnetic Electrode Ⅲ and distal reference Electrode Ⅳ due to the spin dependent electrochemical potential difference. The non-local voltage is determined by the magnetization configuration of Electrodes Ⅱ and Ⅲ[12, 14, 25] and thus can be modulated by an in-plane magnetic field as the electrodes would have different coercivity.

For the case of a forward sweep magnetic field, the magnetization configuration of Electrodes Ⅱ and Ⅲ held parallel before 250 Oe. When the magnetic field turned to be larger than 250 Oe, the magnetization configuration of the two electrodes would be anti-parallel due to the larger coercivity of electrode Ⅱ. Since the positive magnetic field was strong enough (~600 Oe) to rotate the magnetization of electrode Ⅱ, the magnetization configuration returned to the parallel state. The situation in the opposite magnetic field sweep direction was similar. As a result, two magnetoresistance (voltage divides injection current) peaks appear in the range of the in-plane magnetic field ±(250–600) Oe as shown in Fig. 3(a). The red and black lines indicate the forward and reverse sweep of the in-plane magnetic field, respectively.

To quantitatively judge the quality of the spin tunneling junctions, the spin injection efficiency was evaluated by the following approach. First, the magnetoresistance ratio (MR) is calculated by the equation as[12, 14]

$$\mathrm{MR} = \frac{R_{\uparrow\downarrow} - R_{\uparrow\uparrow}}{R_{\uparrow\uparrow}} = \frac{V_{\uparrow\downarrow} - V_{\uparrow\uparrow}}{V_{\uparrow\uparrow}}, \quad (1)$$

where $V_{\uparrow\downarrow}$ and $V_{\uparrow\uparrow}$ are the detected non-local spin voltage under different magnetization configurations and the magnetoresistance $R_{\uparrow\downarrow}$ ($R_{\uparrow\uparrow}$) equals to $V_{\uparrow\downarrow}/I_{inject}$ ($V_{\uparrow\uparrow}/I_{inject}$). The subscripts ↑↓ and ↑↑ indicate the anti-parallel and parallel magnetization configuration of Electrodes Ⅱ and Ⅲ, respectively. Next, the MR can also be valuated as[12, 14]

$$\mathrm{MR} = \frac{(\beta - 1)^2}{4\beta}, \quad (2)$$

when the channel length L approaches zero, and $\beta = \frac{R_{\downarrow TB}}{R_{\uparrow TB}}$ is defined as the spin selectivity of the tunneling barrier. Finally, the spin injection efficiency Π_{inject} can be derived from $\Pi_{inject} = \frac{\beta - 1}{\beta + 1}$[12, 14]. It is worth noting that, the spin injection efficiency defined here is a parameter to calibrate the tunneling process.

According to Eq. (1), an MR of 4.7% was obtained for the channel length L = 400 nm at 1.7 K. By taking this ratio into Eq. (2), the spin injection efficiency of 21% was obtained. It is

worth noting that, the extracted MR is presumably larger than 4.7% when the channel length L approaches 0 because the spin polarization will be relaxed during spin transport. In this situation, the actual spin injection efficiency of the Schottky tunneling contact should be more than 21% at 1.7 K[14].

Next, the dependence of the detected non-local spin voltage on bias was given to exclude the impacts of interface states in the space-charge region. As depicted in Fig. 3(b), the voltage peaks are always restricted the range of ±(250–600) Oe at various injection currents, thus demonstrating that the non-local voltage measured here is not a spurious signal originating from thermal disturbances or background noises. At the same time, the non-local voltage is approximately linear with the injection current, similar to the situations based on metal[26], graphene[27] and Si[28], but unlike that for GaAs accompanied by localized electrons in bands near the surface[29]. Moreover, the magnetoresistance difference $\Delta R = R_{\uparrow\downarrow} - R_{\uparrow\uparrow}$ is extracted from Fig. 3(b) and plotted as a function of the injection current in Fig. 3(c). Obviously, a weak correlation between ΔR and injection current is obtained, which clearly demonstrates the direct tunneling process. Theoretically, ΔR is expressed as[30]

$$\Delta R = \frac{\Delta V}{I_{\text{inject}}} = \frac{P^2 \rho \lambda_s}{A} \exp\left(\frac{-L}{\lambda_s}\right), \tag{3}$$

where P is the spin injection polarization, ρ is the resistivity of the GaN channel, A is the cross-section area and λ_s is the spin diffusion length of the sample. As revealed in Eq. (3), ΔR is determined by the spin injection polarization and spin diffusion length which both are greatly affected by the tunneling process. When the spin-polarized electrons are injected into the space-charge region of the Schottky contact, the spin diffusion length will be reduced due to the band bending induced Rashba spin-orbit coupling through D'yakonov-Perel' spin relaxation mechanism[19]. The spin injection polarization will also be depressed when some of the injected spin-polarized electrons are trapped by the interface states. A large injection current was found to help the trapped electrons escaping from the localized interface states[19]. Therefore, ΔR will increase with increasing injection current when interface-states-assisted tunneling process dominates. As shown in Fig. 3(c), a weak dependence between ΔR and injection current is observed, in contrast to the aforementioned assumption, thus demonstrating a direct tunneling through the Schottky tunneling barrier. This conclusion is consistent with the results from the two-terminal conductance measurements as discussed above.

In contrast from the injection current independent spin signals, ΔR decreases with increasing temperature as shown in Fig. 3(d). This temperature dependence of the magnetoresistance peaks can be attributed to the following possible reasons. First, the increasing temperature will aggravate the spin relaxation rate via D'yakonov-Perel' spin relaxation mechanism. The relaxation rate can be expressed as $\gamma_{\text{DP}} \propto \tau_p(AT - BT^2 + CT^3)$, where τ_p is the momentum relaxation time, and A, B and C are the parameters related to the spin-orbit coupling[31, 32]. As a result, the spin diffusion length $\lambda_s = \sqrt{D\tau_s}$ will be affected, where τ_s is the spin relaxation time and D is the diffusion coefficient. According to Eq. (3), ΔR, as a function of λ_s, will decrease with increasing temperature, consistent with the experimental results shown in Fig. 3(d). However, previous spin dynamics research shows that spin relaxation time will not change much with temperature within 2–10 K to reduce ΔR by nearly half (2.0 → 1.2 mΩ) as shown in Fig. 3(d)[31], and therefore this explanation may not be the sole mechanism. Second, the signal-to-noise ratio gets worse quickly with increasing temperature and the magnetoresistance can't be clearly distinguished as the temperature exceeds 10 K. Hence, the signal extraction of ΔR is affected near 10 K. Further theoretical and experimental research is needed to elucidate the origin of the observed temperature dependence of the spin magnetoresistance.

4. Conclusions

In conclusion, electrical spin injection and detection were demonstrated in a heavily doped n-GaN with Co/GaN Schottky tunneling contacts at low temperature. The spin injection efficiency was 21% at 1.7 K. It is demonstrated that the direct tunneling is dominant by non-local magnetoresistance measurements, which is in good agreement with the weak dependence of the zero-bias resistance on temperature. Finally, the dependence of the magnetoresistance on temperature has also been preliminarily discussed.

Acknowledgements

This work was supported by the National Key Research and Development Program of China (Nos. 2022YFB3605604, and 2018YFE0125700) and the National Natural Science Foundation of China (Nos. 62225402, 61927806, 62234001, and U22A2074). The authors are grateful for the technical support for Nano-X from Suzhou Institute of Nano-Tech and Nano-Bionics, Chinese Academy of Sciences (SINANO), Chinese Academy of Sciences.

References

[1] Datta S, Das B. Electronic analog of the electro-optic modulator. Appl Phys Lett, 1990, 56, 665
[2] Schliemann J, Egues J C, Loss D. Nonballistic spin-field-effect transistor. Phys Rev Lett, 2003, 90, 146801
[3] Thompson S E, Parthasarathy S. Moore's law: The future of Si microelectronics. Mater Today, 2006, 9, 20
[4] Dhar S, Brandt O, Ramsteiner M, et al. Colossal magnetic moment of Gd in GaN. Phys Rev Lett, 2005, 94, 037205
[5] Dietl T, Ohno H, Matsukura F, et al. Zener model description of ferromagnetism in zinc-blende magnetic semiconductors. Science, 2000, 287, 1019
[6] Yin C M, Shen B, Zhang Q, et al. Rashba and Dresselhaus spin-orbit coupling in GaN-based heterostructures probed by the circular photogalvanic effect under uniaxial strain. Appl Phys Lett, 2010, 97, 181904
[7] Zhang S X, Tang N, Zhang X Y, et al. Excitonic effects on electron spin orientation and relaxation in wurtzite GaN. Phys Rev B, 2021, 104, 125202
[8] Johnson M, Silsbee R H. Spin-injection experiment. Phys Rev B, 1988, 37, 5326
[9] Schmidt G, Ferrand D, Molenkamp L W, et al. Fundamental obstacle for electrical spin injection from a ferromagnetic metal into a diffusive semiconductor. Phys Rev B, 2000, 62, R4790
[10] Rashba E I. Theory of electrical spin injection: Tunnel contacts as a solution of the conductivity mismatch problem. Phys Rev B, 2000, 62, R16267

[11] Jaffrès H, Fert A. Spin injection from a ferromagnetic metal into a semiconductor. J Appl Phys, 2002, 91, 8111
[12] Bhattacharya A, Baten M Z, Bhattacharya P. Electrical spin injection and detection of spin precession in room temperature bulk GaN lateral spin valves. Appl Phys Lett, 2016, 108, 042406
[13] Kum H, Heo J, Jahangir S, et al. Room temperature single GaN nanowire spin valves with FeCo/MgO tunnel contacts. Appl Phys Lett, 2012, 100, 182407
[14] Song A K, Chen J J, Lan J S, et al. Modulating room temperature spin injection into GaN towards the high-efficiency spin-light emitting diodes. Appl Phys Express, 2020, 13, 043006
[15] Huang L, Wu H, Liu P, et al. Room temperature spin injection into SiC via Schottky barrier. Appl Phys Lett, 2018, 113, 222402
[16] Hanbicki A T, Jonker B T, Itskos G, et al. Efficient electrical spin injection from a magnetic metal/tunnel barrier contact into a semiconductor. Appl Phys Lett, 2002, 80, 1240
[17] Zube C, Malindretos J, Watschke L, et al. Spin injection in epitaxial MnGa(111)/GaN(0001) heterostructures. J Appl Phys, 2018, 123, 033906
[18] Jönsson-Åkerman B J, Escudero R, Leighton C, et al. Reliability of normal-state current–voltage characteristics as an indicator of tunnel-junction barrier quality. Appl Phys Lett, 2000, 77, 1870
[19] Liu X C, Tang N, Fang C, et al. Spin relaxation induced by interfacial effects in n-GaN/MgO/Co spin injectors. RSC Adv, 2020, 10, 12547
[20] Jiang L, Choi W S, Jeen H, et al. Tunneling electroresistance induced by interfacial phase transitions in ultrathin oxide heterostructures. Nano Lett, 2013, 13, 5837
[21] Wang Y H, Zhang Q, Zhou J L, et al. Fowler–Nordheim tunneling-assisted enhancement of tunneling electroresistance effect through a composite barrier. Appl Phys Lett, 2020, 116, 202901
[22] Jedema F J, Filip A T, van Wees B J. Electrical spin injection and accumulation at room temperature in an all-metal mesoscopic spin valve. Nature, 2001, 410, 345
[23] Jedema F J, Heersche H B, Filip A T, et al. Electrical detection of spin precession in a metallic mesoscopic spin valve. Nature, 2002, 416, 713
[24] van't Erve O M J, Hanbicki A T, Holub M, et al. Electrical injection and detection of spin-polarized carriers in silicon in a lateral transport geometry. Appl Phys Lett, 2007, 91, 212109
[25] Zhou Y, Han W, Chang L T, et al. Electrical spin injection and transport in germanium. Phys Rev B, 2011, 84, 125323
[26] Valenzuela S O, Monsma D J, Marcus C M, et al. Spin polarized tunneling at finite bias. Phys Rev Lett, 2005, 94, 196601
[27] Tombros N, Jozsa C, Popinciuc M, et al. Electronic spin transport and spin precession in single graphene layers at room temperature. Nature, 2007, 448, 571
[28] van 't Erve O M J, Awo-Affouda C, Hanbicki A T, et al. Information processing with pure spin currents in silicon: Spin injection, extraction, manipulation, and detection. IEEE Trans Electron Devices, 2009, 56, 2343
[29] Lou X H, Adelmann C, Crooker S A, et al. Electrical detection of spin transport in lateral ferromagnet–semiconductor devices. Nat Phys, 2007, 3, 197
[30] Jedema F J, Costache M V, Heersche H B, et al. Electrical detection of spin accumulation and spin precession at room temperature in metallic spin valves. Appl Phys Lett, 2002, 81, 5162
[31] Buß J H, Rudolph J, Natali F, et al. Temperature dependence of electron spin relaxation in bulk GaN. Phys Rev B, 2010, 81, 155216
[32] Zhang X Y, Tang N, Yang L Y, et al. Electrical spin injection into the 2D electron gas in AlN/GaN heterostructures with ultrathin AlN tunnel barrier. Adv Funct Mater, 2021, 31, 2009771

Zhenhao Sun got his BS from Nanjing University in 2019. Now he is a Ph.D. student at Peking University. His research focuses on spintronic devices of GaN-based semiconductors.

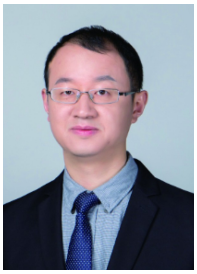

Ning Tang is a professor at School of Physics, Peking University. He received a Ph.D. degree in 2007 from School of Physics, Peking University. His current research mainly focuses on wide band gap semiconductor spintronics.